JOURNAL OF PROPULSION AND POWER
Vol. 19, No. 4, July–August 2003

Deceleration of Supersonic Plasma Flow by an Applied Magnetic Field

Sergei V. Bobashev* and Yurii P. Golovachov*
Russian Academy of Sciences, 194021, St. Petersburg, Russia
and
David M. Van Wie†
Johns Hopkins University, Applied Physics Laboratory, Laurel, Maryland 20723-6099

The problem of gas flow control by a magnetic field is considered as it applies to flows in the intakes of supersonic aircraft. The method to be discussed for control of the intake operation consists of a preliminary ionization of incoming gas and subsequent control of the ionized flow by an applied magnetic field. To estimate the prospects of such a mode for flow control and the effects of the magnetogasdynamic interaction, a numerical investigation was conducted. The results demonstrate the possibility of controlling the flow structure at reasonable plasma and magnetic field parameters. The effects of magnetogasdynamic interaction on supersonic flow deceleration are investigated.

Nomenclature

a_0 = Bohr radius
$\boldsymbol{B}$ = induction of magnetic field
$\boldsymbol{b}$ = unit vector of magnetic induction
c = speed of light
c_i = computational vector
$\boldsymbol{E}$ = electric field strength
e = charge of electron
$\boldsymbol{j}$ = electric current density
k = Boltzman constant, external load coefficient
k_i = ionization rate constant
k_r = recombination rate constant
L = flow length scale
l_D = Debye length
M = Mach number
m = heavy particle mass
m_e = mass of electron
n_e = electron number density
$\dot{n}_e$ = number rate of electron production per unit volume
n_α = number density of the α component
P = plasma pressure
Re_m = magnetic Reynolds number
S = Stuart number
s = ion slip parameter
T = heavy particle temperature
T_c = electron temperature
$\boldsymbol{V}$ = mass-averaged flow velocity
v, σ = volume and surface of computational cell
α = ionization degree
β = Hall parameter
ε = permittivity
ε_{ion} = ionization energy per atom
μ = permeability
ν_{ea} = collision frequency of electron with atoms
ν_{ei} = collision frequency of electron with ions
ρ = plasma density
σ = electric conductivity
$\boldsymbol{\sigma}$ = tensor of electric conductivity
φ = electric field potential
ω_p = plasma frequency

Received 29 March 2002; revision received 8 February 2003; accepted for publication 23 February 2003.

*Professor, Ioffe Physico-Technical Institute, 26 Polytechnicheskaya.
†Supervisor, Aeronautical Science and Technology Group, 11100 Johns Hopkins Road, Associate Fellow AIAA.

Introduction

THE idea of controlling electrically conducting flows with an applied magnetic field is successfully exploited in a number of technical applications. Until recently, the efforts of researchers have been concentrated, for the most part, on the investigation of magnetohydrodynamic (MHD) flows in ground-based facilities intended for the transformation of thermal energy to electric energy. This paper considers the prospects of the idea as it applies to supersonic aerodynamics problems and, more exactly, to the control of flows in the intakes of supersonic aircraft. The use of MHD technology is an important element of the AJAX concept for supersonic aircraft.[1,2] In particular, an applied magnetic field is assumed to be used for development of controlled intakes, which would sustain the design operating regime with variation of the flight conditions.[3–5]

The MHD effects on the flow structure are determined by the electrical conductivity and by the induction of a magnetic field. Some techniques for obtaining sufficient ionization of the incoming stream are discussed in Refs. 6–8. Our investigation is focused on MHD flow control. To separate this problem from that of flow ionization, the calculations are carried out with rare gas plasmas that are characterized by far slower recombination times as compared with airflow. The use of rare gas plasma is an important simplification that is made to maintain the necessary level of the electric conductivity and to allow investigation of the flow control potential. Numerical simulations of the plasma flows are carried out within the MHD approach using high-resolution Godunov-type computational schemes.

Formulation of the Problem

Preliminary estimates of magnetogasdynamic interaction and the prospects of flow control were carried out with the simplest magnetohydrodynamic interaction (MHI) model, in which the weakly ionized plasma was considered as a perfect gas with constant heat capacity and electrical conductivity. After preliminary calculations with the simplest model, the physical model was refined through specification of real thermodynamic and electrophysical properties of a nonequilibrium rare gas plasma.

Basic Assumptions and Governing Equations

The calculations are carried out within the framework of the MHD approach, with the induced magnetic field neglected. When the refined physical model is used, the partially ionized rare gas plasma is assumed to consist of atoms a, singly ionized positive ions i, and electrons e. The analysis is conducted with a two-temperature model and under the assumption of plasma quasi neutrality. Validity of the preceding assumptions follows from inequalities $l_D \ll L$, $V_0 \ll c$, $E_0 < V_0 B_0$, $L/V_0 \gg \omega_p^{-1}$, and $Re_m < 1$, which certainly hold for the flows under study. Here, $l_D = \sqrt{\varepsilon k T_e / n_e e^2}$ is the debye length, $\omega_P = \sqrt{n_e e^2/\varepsilon m_e}$ is the plasma frequency, and $Re_m = V_0 L \sigma \mu$ is the magnetic Reynolds number. The subscript 0 denotes the reference scales for gas velocity, electric field strength, and induction of the magnetic field. In addition, we neglect the viscosity, heat conductivity, and diffusion, which allows us to use an inviscid gas model as described by the Euler equations. The latter assumption is substantiated, to some extent, by the high Reynolds numbers of the flows under study, but it precludes an analysis of situations with flow separation.

With the preceding assumptions, the nonequilibrium three-component and two-temperature plasma flow subjected to an applied magnetic field is governed by the following equations:
The total continuity equation is

$$\frac{\partial \rho}{\partial t} + \nabla \cdot (\rho \boldsymbol{V}) = 0 \tag{1}$$

The continuity equation for the electrons is

$$\frac{\partial n_e}{\partial t} + \nabla \cdot (n_e \boldsymbol{V}) = \dot{n}_e \tag{2}$$

The total momentum balance equation is

$$\frac{\partial \rho \boldsymbol{V}}{\partial t} + \nabla \cdot (\rho \boldsymbol{V}\boldsymbol{V} + P) = \boldsymbol{j} \times \boldsymbol{B} \tag{3}$$

The total energy balance equation is

$$\frac{\partial}{\partial t}\left(\frac{\rho V^2}{2} + \frac{3}{2}P\right) + \nabla \cdot \left[\left(\frac{\rho V^2}{2} + \frac{5}{2}P\right)\boldsymbol{V}\right] = \boldsymbol{j} \cdot \boldsymbol{E} - \dot{n}_e \varepsilon_{\text{ion}} \tag{4}$$

The energy balance equation for the electrons is

$$\frac{\partial}{\partial t}\left(\frac{3}{2}P_e\right) + \nabla \cdot \left(\frac{5}{2}P_e \boldsymbol{V}\right) = \boldsymbol{V} \cdot \nabla P_e + \boldsymbol{j} \cdot (\boldsymbol{E} + \boldsymbol{V} \times \boldsymbol{B}) - \dot{n}_e \varepsilon_{\text{ion}}$$

$$- 3\frac{m_e}{m} k n_e (\nu_{\text{ei}} + \nu_{ea})(T_e - T) \tag{5}$$

Here, $\rho = \rho_a + \rho_i + \rho_e$ is the plasma density, $p = p_a + p_i + p_e$ the plasma pressure, $p_\alpha = n_\alpha k T_\alpha$ the partial pressure of the α component ($\alpha = a, i, e$), n_α is the number density of the α component, and $m = m_a \approx m_i$ is the mass of a heavy particle.

In the case of steady supersonic flows, the boundary conditions for Eqs. (1–5) are formulated with all plasma parameters prescribed on the inflow boundary and impermeability conditions imposed on the duct walls.

Ionization Kinetics and Collision Frequencies

The main processes that determine the charged particle concentrations within the range of conditions considered are ionization by electron impact and three-particle recombination,[9]

$$A + e \Leftrightarrow A^+ + e + e$$

which implies the following definition for the number rate of the electron production

$$\dot{n}_e = k_i n_e n_a - k_r n_e^3$$

The recombination rate constant k_r is calculated after the theory of nonequilibrium ionization in a low-temperature rare gas plasma, developed by Biberman et al.[10] The ionization rate constant k_i is found through the equilibrium constant.

Collision frequencies are evaluated with formulas[11,12]

$$\nu_{\text{ei}} = 3.64 \times 10^{-6} n_e \left(\ell n \Lambda / T_e^{\frac{3}{2}}\right)(s^{-1})$$

$$\Lambda = 1.24 \times 10^7 \sqrt{T_e^3 / n_e}$$

$$\nu_{ea} = \tfrac{4}{3}\sigma_{ea} n_a \sqrt{(8kT_e/\pi m_e)}(s^{-1})$$

where

$$\sigma_{ea} = a_0^2\left(-0.535 + 1.46 \times 10^{-3} T_e\right)$$

for Ar and

$$\sigma_{ea} = a_0^2\left(-1.82 + 2.2 \times 10^4 T_e^{-1} + 3.8 \times 10^{-7} T_e^2\right)$$

for Xe, where $a_0 = 0.529 \times 10^{-10}$ m is the radius of first Bohr orbit.

MHI Models

Ignoring the induced magnetic field, one can take magnetic induction to be that of the applied magnetic field. The latter being known, the electric current density and the electric field strength remain to be determined to calculate the ponderomotive force and Joule heat release. With that end in view, one can use the generalized Ohm's law

$$\boldsymbol{j} + \beta_e \boldsymbol{j} \times \boldsymbol{b} = \sigma[\boldsymbol{E} + \boldsymbol{V} \times \boldsymbol{B} + (\nabla P_e / e n_e)] \tag{6}$$

in which the electric field strength may be found through specification of the external load coefficient k:

$$\boldsymbol{E} = -k(\boldsymbol{V} \times \boldsymbol{B})$$

Here, $\sigma = n_e e^2/m_e(\nu_{\text{ei}} + \nu_{ea})$ is the electrical conductivity and $\beta_e = eB/m_e(\nu_{\text{ei}} + \nu_{ea})$ is the Hall parameter for the electrons. The preceding MHI model is widely used in calculations of MHD generators.[13]

A more accurate way to determine the electric field strength comes from the use of Maxwell equations. In the case of a stationary magnetic field, the Faraday law reads

$$\nabla \times \boldsymbol{E} = 0$$

which implies that

$$\boldsymbol{E} = -\nabla \varphi$$

The generalized Ohm's law is rewritten in the form

$$\boldsymbol{j} = \tilde{\sigma}[-\nabla \varphi + \boldsymbol{V} \times \boldsymbol{B} + (\nabla P_e / e n_e)] \tag{7}$$

The electric field potential is found from the condition $\nabla \cdot \boldsymbol{j} = 0$, which follows from Maxwell equations. Along with Eq. (7), this yields the equation

$$\nabla\{\tilde{\sigma}[-\nabla \varphi + \boldsymbol{V} \times \boldsymbol{B} + (\nabla P_e / e n_e)]\} = 0 \tag{8}$$

for the electric field potential.

Wall boundary conditions for Eq. (8) are given by a fixed voltage on the electrodes and by a zero electric current normal to any insulated segments of the wall. The inflow and outflow boundary conditions depend on the duct geometry and the electrode system design. Calculations conducted with the preceding MHI models have shown that the algebraic model provides qualitatively correct results, but slightly overestimates flow deceleration by the applied magnetic field.[5]

Numerical Method

The method for solving Eqs. (1–5) is based on the Godunov-type high-resolution finite volume scheme.[14] Stationary solutions are obtained via a time-asymptotic technique. The calculations were performed for planar flows. In this case, the computational procedure

looks as follows. The governing equations are written for the Cartesian coordinates (x, y) in the form

$$\frac{\partial U}{\partial t} + \frac{\partial F}{\partial x} + \frac{\partial G}{\partial y} = H + R \tag{9}$$

where

$$U = \begin{Bmatrix} \rho \\ n_e \\ \rho V_X \\ \rho V_Y \\ \dfrac{\rho V^2}{2} + \dfrac{3}{2}P \\ \dfrac{3}{2}P_e \end{Bmatrix}, \qquad F = \begin{Bmatrix} \rho V_X \\ n_e V_X \\ \rho V_X V_X + p \\ \rho V_Y V_X \\ \left(\dfrac{\rho V^2}{2} + \dfrac{5}{2}P\right) V_X \\ \dfrac{5}{2}P_e V_X \end{Bmatrix}$$

$$G = \begin{Bmatrix} \rho V_Y \\ n_e V_Y \\ \rho V_X V_Y \\ \rho V_Y V_Y + P \\ \left(\dfrac{\rho V^2}{2} + \dfrac{5}{2}P\right) V_Y \\ \dfrac{5}{2}P_e V_Y \end{Bmatrix}, \qquad R = \begin{Bmatrix} 0 \\ 0 \\ 0 \\ 0 \\ 0 \\ \boldsymbol{V} \cdot \nabla P_e \end{Bmatrix}$$

$$H = \begin{Bmatrix} 0 \\ \dot{n}_e \\ (\boldsymbol{j} \times \boldsymbol{B})_X \\ (\boldsymbol{j} \times \boldsymbol{B})_Y \\ \boldsymbol{j} \cdot \boldsymbol{E} - \dot{n}_e \varepsilon_{\text{ion}} \\ \boldsymbol{j} \cdot (\boldsymbol{E} + \boldsymbol{V} \times \boldsymbol{B}) - \dot{n}_e \varepsilon_{\text{ion}} - 3\dfrac{m_e}{m} k n_e \left(\nu_{\text{ei}} + \nu_{ea}\right)\left(T_e - T\right) \end{Bmatrix}$$

Assuming gasdynamic variables to be constant within a computational cell, and making use of the integral formula of vector analysis, one can write out the finite volume notation of Eq. (9) for a computational cell

$$\frac{\mathrm{d}U}{\mathrm{d}t} = -\frac{1}{\nu}\int_{\sigma} \left(F^n n_x + G^n n_y\right) \mathrm{d}s + H + R^n \tag{10}$$

where ν and σ are the volume and the surface of a computational cell, n_x and n_y are the projections of the unit vector that is normal to surface σ, and superscript n denotes the values at the preceding time level $t = t^n$. Integration over a cell surface is fulfilled with formula

$$\int_{\sigma} (Fn_X + Gn_Y)\,\mathrm{d}s = (F_n)_{i+\frac{1}{2},j} + (F_n)_{i-\frac{1}{2},j} + (F_n)_{i,j+\frac{1}{2}} + (F_n)_{i,j-\frac{1}{2}} \tag{11}$$

where subscript n corresponds to the normal to a cell side. The fluxes are given by the formula

$$F_n = \begin{Bmatrix} \rho V_n \\ n_e V_n \\ \rho V_n V_x + p n_x \\ \rho V_n V_y + p n_y \\ \left(\dfrac{\rho V^2}{2} + \dfrac{5}{2}p\right) V_n \\ \dfrac{5}{2}p_e V_n \end{Bmatrix}$$

When the fluxes F_n are evaluated, the gasdynamic functions are found from the solution of the Riemann problem with the following initial data:

$$U^L_{i+\frac{1}{2},j} = U_{i,j} + \nabla U_{i,j} \cdot \boldsymbol{c}_1, \qquad U^R_{i+\frac{1}{2},j} = U_{i+1,j} + \nabla U_{i+1,j} \cdot \boldsymbol{c}_2 \tag{12}$$

where $\boldsymbol{c}_1$ and $\boldsymbol{c}_2$ are the vectors drawn from the centers of the neighboring computational cells to the middle of their boundary. Similar formulas are used on other sides of a computation procedure, for example:

$$\left(\frac{\mathrm{d}U}{\mathrm{d}x}\right)_{i,j} = \min \mathrm{mod}\left(\frac{U_{i,j} - U_{i-1,j}}{\Delta x}, \frac{U_{i+1,j} - U_{i,j}}{\Delta x}\right) \tag{13}$$

With known fluxes, F and G and the components of vector R, which are evaluated with the earlier time level data, Eqs. (10) represent the set of ordinary differential equations. This set is integrated in time with a two-step implicit scheme. The preceding computational procedure is second-order accurate with respect to both spatial coordinates in the flow regions with smooth function behavior. Computations were performed with the grids, which included 64 nodes across the duct and 300–400 nodes along the duct. The admissible time increment is limited by the Courant–Friedrichs–Lewy stability condition to maintain the accuracy of the time-dependent development of the flowfield. This method has also been modified to conduct space-marching computations of supersonic flows for steady flows and was also generalized for solving three-dimensional problems[5]. Poisson equation (8) for the electric field potential is solved by use of the implicit/explicit line relaxation procedure,[15] which includes the Thomas algorithm in the y direction. The stationary flows were calculated until the residual for the electric field potential became less than 10^{-6}.

Results

Computational predictions of the flowfield through a planar inlet with MHD interactions have been conducted for a geometry that is being investigated in a parallel experimental effort.[16] A schematic of the working section of the experimental setup is shown in Fig. 1, with dimensions provided in millimeters. A shock tube is used to produce a reservoir of high-temperature plasma that is expanded through a planar converging–diverging nozzle to approximately Mach 4 conditions. With Krypton used as the test gas, typical reservoir conditions were at $T = 9800$ K and $\rho = 1.08$ kg/m^3. The supersonic plasma flow produced at the nozzle is characterized by $T = 1550$ K, $\rho = 0.0645$ kg/m^3, and $\sigma = 600$ S/m. The simulated inlet consists of opposing compression surfaces with 5.4-deg ramps. Flush-mounted electrodes are located near the aft end of the nozzle and on the compression surfaces. A pulsed magnetic field with an induction value up to 1.5 T is applied normal to the plane of Fig. 1, which results in the flows under study being planar both with and without the MHI.

Preliminary Estimates

Preliminary estimates of the MHD effects on plasma flows were performed with the simplest physical model of a perfect gas, in

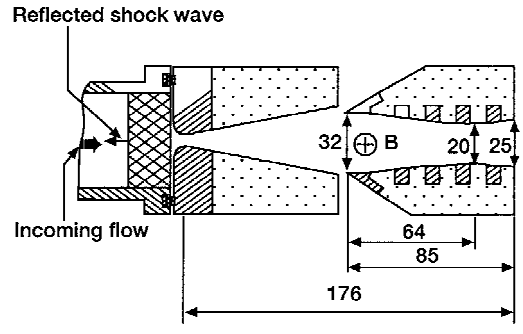

Fig. 1 Outline of the experimental setup, including nozzle and inlet.

which the specific heat ratio γ and the electrical conductivity σ are assumed to be constant, as is the induction of the applied magnetic field B. This being the case, the MHI is characterized by the Stuart number $S = \sigma B^2 L/\rho_0 V_0$, the Hall parameter β, and either the external load coefficient k or the electrode voltage $\Delta\varphi$, depending on the MHI model exploited. The MHD flows in the diffuser model are investigated with the inflow parameters obtained from a preliminary calculation of the nozzle flow. The distribution of the electric field potential on the inflow boundary is obtained from linear interpolation between the fixed values on the lower and upper electrodes. Note that near-electrode sheath effects are neglected in the present formulation. The outflow boundary condition for the electric field potential is taken to be $\partial\varphi/\partial x = 0$, which accounts for the rapid diminution of the electric field with the distance from the electrodes.

Figure 2 presents an example of the computational results. The pressure and the electric field potential are normalized by $\rho_0 V_0^2$ and by $V_0 L B$, where subscript 0 denotes gas parameters at the critical cross section of the nozzle, and x and y are provided in millimeters. Figure 2d shows only direction, but not magnitude, of the electric current density. Note that the Stuart number S is defined here with the length scale $L = 1$ mm, which is much shorter than the actual length of the model ($L = 85$ mm). Note that the MHD flow presented in Fig. 2 is supersonic throughout the diffuser model.

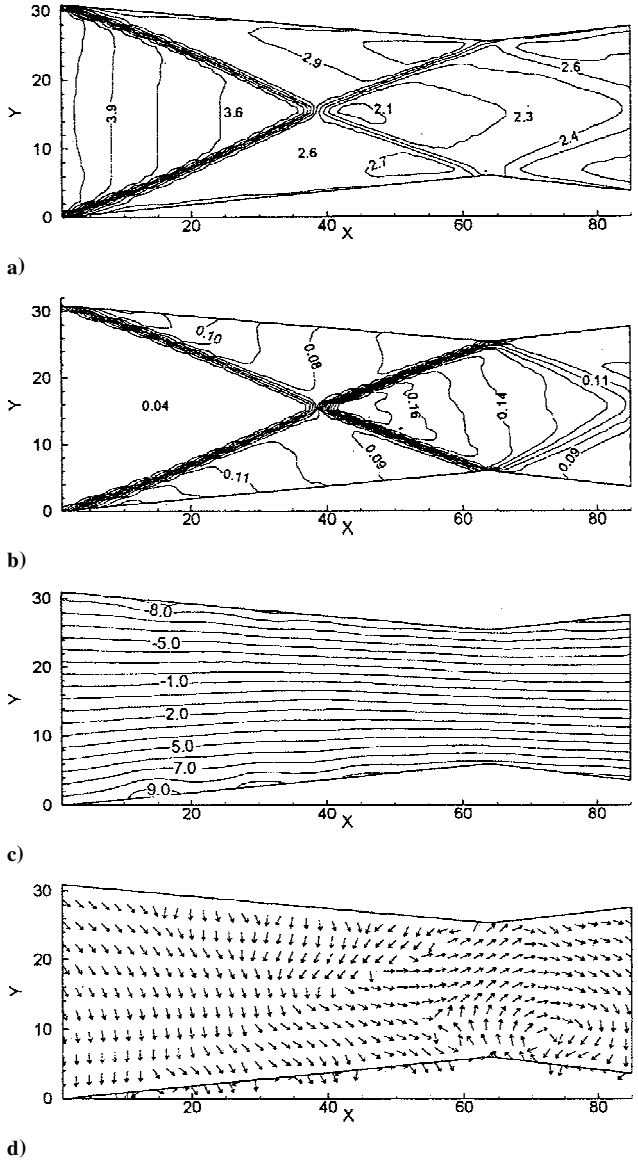

Fig. 2 MHD flow in the diffuser model; $S = 0.006$, $\beta = 0.5$, and $\Delta\varphi = 18$: a) Mach number contours b) static pressure contours, c) contours of electric field potential, and d) electric current map.

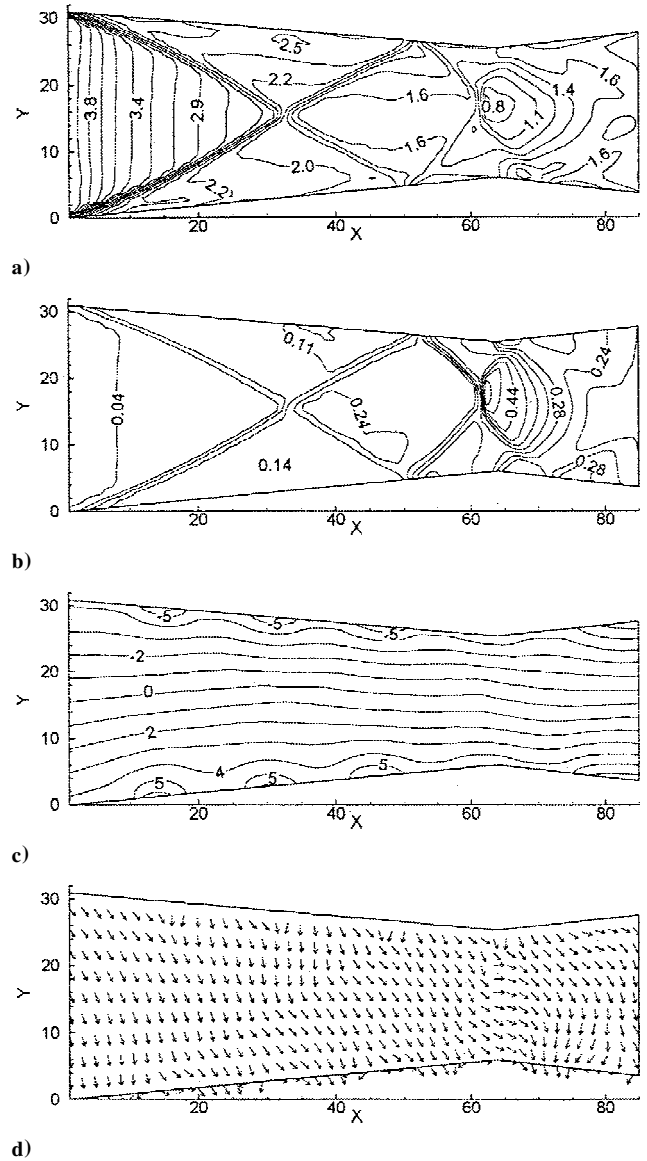

Fig. 3 MHD flow in the diffuser model; $S = 0.006$, $\beta = 0.5$, $\Delta\varphi = 9$: a) Mach number contours, b) static pressure contours, c) contours of electric field potential, and d) electric current map.

Figure 3 shows the drastic change of the flow structure that occurs with a decrease of the electrode voltage, which results in an increase in the electric current density and, consequently, an increase in the pondermotive force and Joule heat release. In Figs. 3a and 3b, which present the Mach number and the static pressure contours, one can see a normal shock and a small subsonic zone within the diffuser model. In Figs. 3c and 3d, a noticeable distortion of isolines of the electric field potential and the disappearance of the electric current vortices are seen.

Figure 4 demonstrates the effects of MHI parameters on the Mach number, static pressure, and total pressure ratio at the outlet of the diffuser model. The total pressure ratio, P_t/P_{t0}, which is an important characteristic of a supersonic intake, is defined as the ratio of the outflow and inflow total pressures. The dashed curves present calculations without the magnetic field. One can see the important role of the electrode voltage, in Fig. 4. An increase of the Hall parameter deteriorates flow deceleration, resulting in lower static pressure and a slight reduction of the total pressure loss. An increase of the Stuart number affects the MHD flow in the opposite way. The results presented in Fig. 4c show that plasma deceleration by the applied magnetic field is accompanied by a substantial

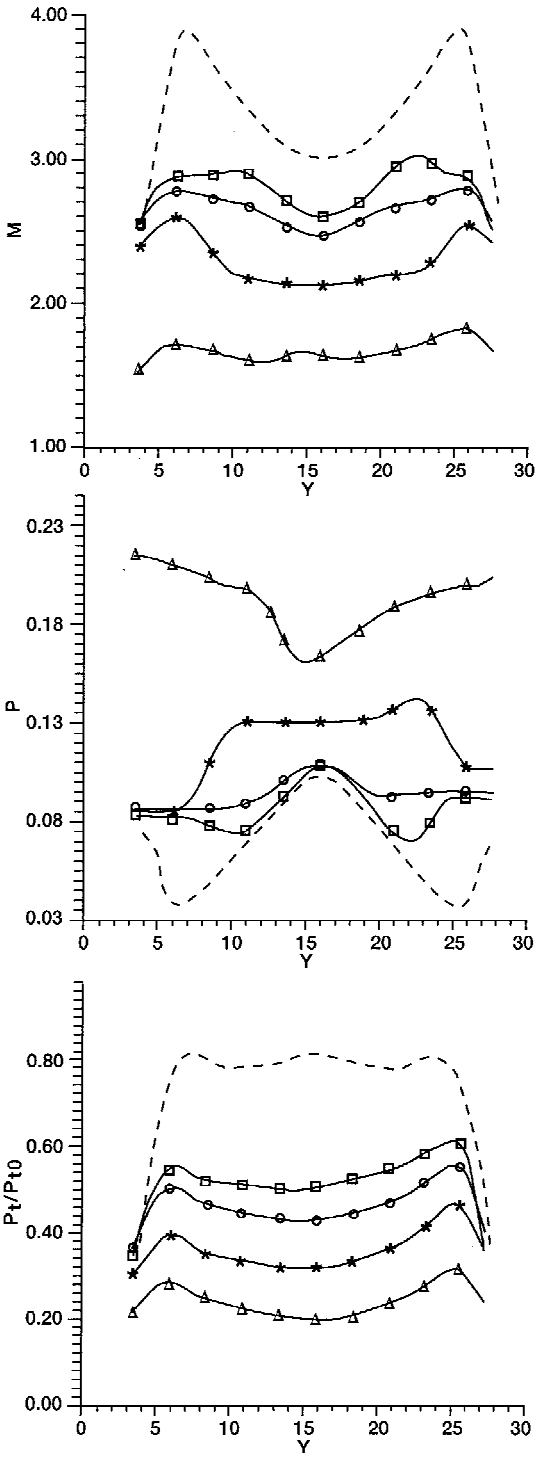

Fig. 4 Distributions of Mach number, static pressure, and total pressure ratio at the outlet of the diffuser model: ----, without magnetic field; ○: $S = 0.006$, $\beta = 0.5$, and $\Delta\varphi = 18$; □: $S = 0.006$, $\beta = 1.0$, and $\Delta\varphi = 18$; △: $S = 0.006$, $\beta = 0.5$, and $\Delta\varphi = 9$; and ∗: $S = 0.012$, $\beta = 0.5$, and $\Delta\varphi = 18$.

loss of the total pressure, with only a moderate increase in the static pressure level. This conclusion agrees with previous analytical estimates.[17]

A comparison of calculations with the experimental data is provided in Fig. 5. Shown is the distance of the intersection of oblique shocks issuing from the leading edges of the diffuser walls vs induction of the applied magnetic field. The axial distance x_c is measured from the diffuser inlet. With increasing MHI, the intersection point moves upstream, that is, x_c decreases. The results of calculations and measurements are depicted by the solid line and by the circles,

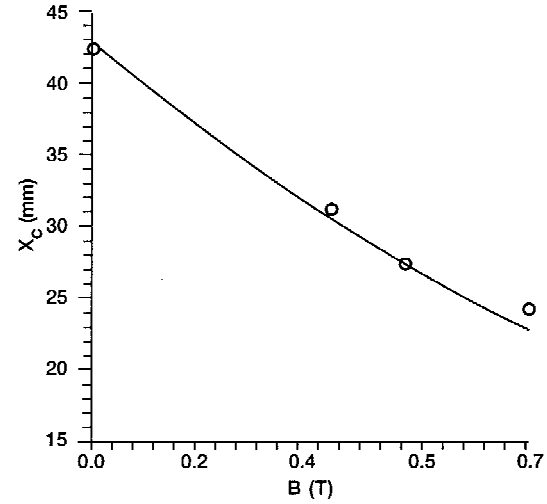

Fig. 5 Position of the shock intersection point vs induction of applied magnetic field: ——, computations and ○, experiment.

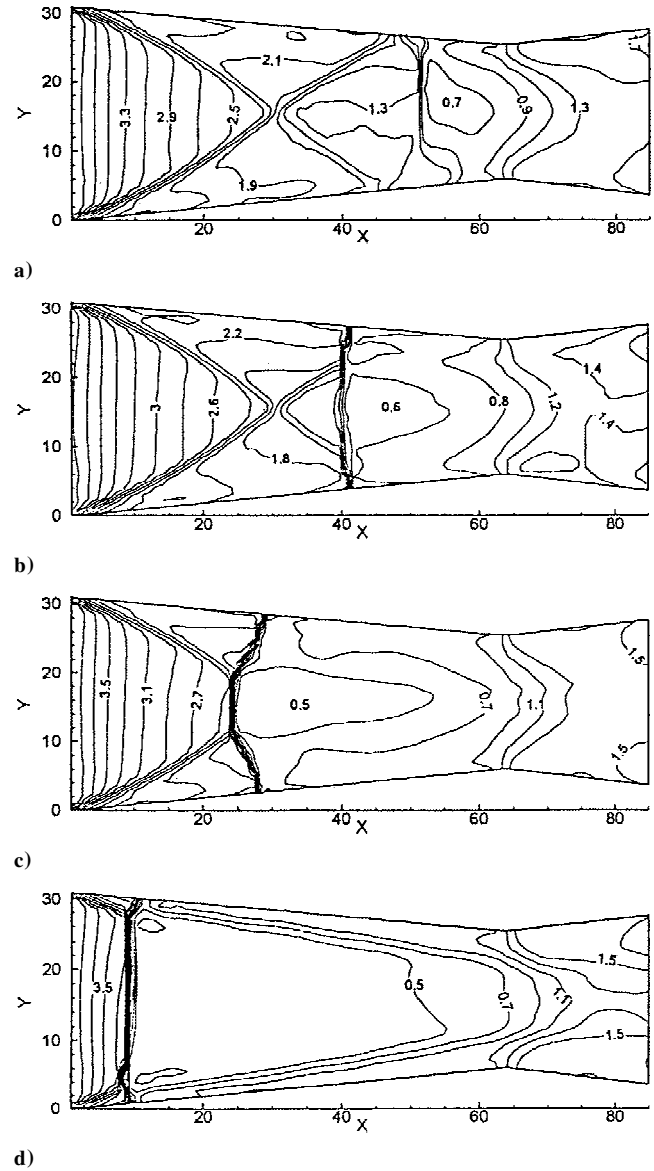

Fig. 6 Time history of Mach number contours in diffuser model; $S = 0.006$, $\beta = 0.5$, and $\Delta\varphi = 6$.

respectively. The conductivity was not well known in the experiments, and so the relationship between the induction of applied magnetic field B and the Stuart number S used in the calculations was established by locating one of the experimental points on the calculated curve. One can see surprisingly good agreement between the experimental data and calculations, in spite of the use of a rather crude physical model.

As the MHI is increased, the flow under study eventually becomes nonstationary, corresponding to an effective unstart of the intake with formation of a normal shock that moves upstream toward the diffuser leading edge, followed by an extensive subsonic zone. Figure 6 presents the Mach number contours in such an unsteady flow for several consecutive moments that follow one after another through 2000 time steps. In this case, the unsteady flow regime was achieved by a reduction of the electrode voltage.

The results of the numerical simulation indicate a substantial loss of the total pressure when plasma flow is decelerated by an applied magnetic field. For this reason, it seems expedient to use MHI within a small part of the duct to provide the optimum flowfield structure. Apart from the expected savings in the total pressure, this would simplify significantly the problems of ionization and creation of an applied magnetic field. The preceding idea was estimated with reference to planar MHD flows in the supersonic intake shown in Fig. 7, which was designed for the forebody shocks intersecting the cowl lip at $M_0 = 6$. The magnetic field is applied along the z axis, which is normal to the plane of the intake. The calculations have been carried out for the case of the Faraday MHD generator with continuous electrodes by the use of the algebraic MHI model. Figures 7a and 7b show the flowfield structure, which includes the shock waves and expansion fans arising from the wall slope discontinuities. On the upper wall, a reflected shock appears and, having interacted with the expansion fan, it intersects and reflects from the bottom wall. Figure 7a presents the results for off-design Mach number, $M_0 = 7$. Figure 7b corresponds to the flow with the same Mach number, $M_0 = 7$, subjected to an applied magnetic field. The magnetic field acts only within a small region corresponding to the Stuart number distribution shown in Fig. 7c. The results display a recovery of the flowfield structure inherent in the design operating condition in which the shocks arising from the lower wall slope discontinuities meet at the cowl lip.

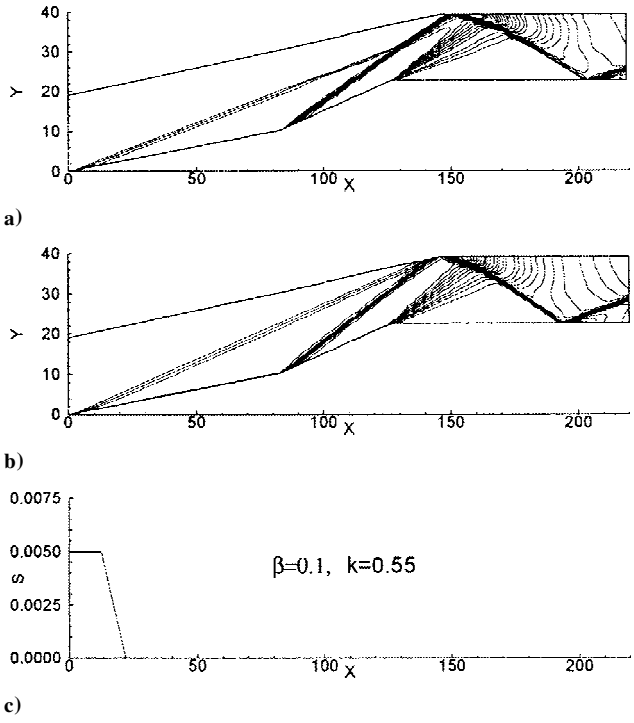

Fig. 7 Density contours in supersonic intake at Mach 7: a) without magnetic field and b) with magnetic field; c) Stuart number distribution.

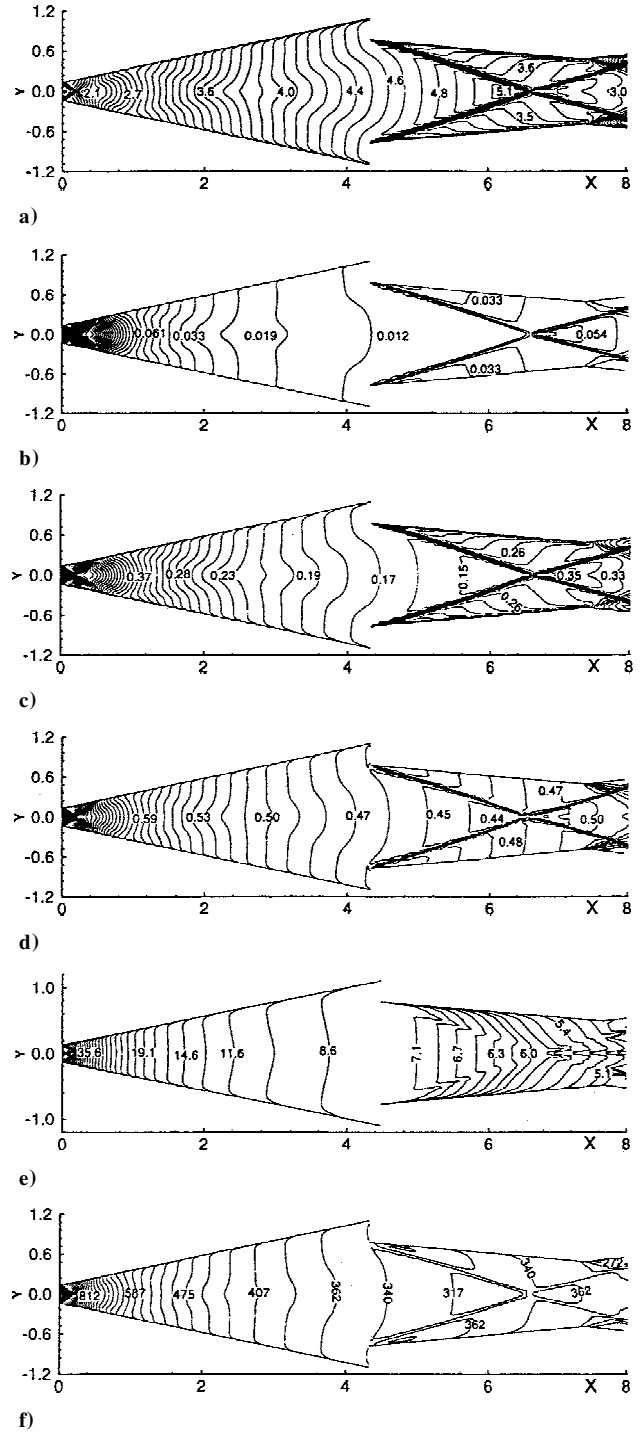

Fig. 8 Contours of a) Mach number, b) static pressure, c) heavy particle temperature, d) electron temperature, e) ionization degree, and f) electric conductivity with no magnetic field.

The results of numerical simulation allow one to estimate the plasma parameters required for the considered mode of flow control. For example, with the length scale $L = 1$ cm, magnetic induction $B = 2$ T, Mach number $M_0 = 6$, and density $\rho = 0.2$ kg/m^3 (which corresponds to the altitude $H = 15$ km), the Stuart number ensuring a desirable change of the shock structure is achieved at plasma electric conductivity σ on the order of tens of mho/m.

Nonequilibrium MHD Flows

The results presented hereafter were obtained with the refined physical model, which took into account nonequilibrium ionization and the real electrophysical properties of shock-heated argon plasma. The main objectives of these calculations are evaluation

of the ionization degree, the electric conductivity of plasma, the Hall parameter, and the investigation of the effects of variable electrophysical properties on plasma flow deceleration caused by the applied magnetic field. Plasma parameters in the critical cross section of the nozzle are the following: $M = 1.00$; $T = T_0 = 8600$ K; $T_e = 10{,}000$ K; $\alpha = 6.28 \times 10^{-3}$; and $n_a + n_i = n_0 = 10^{25}\text{m}^{-3}$ The Mach number is evaluated with the mass-averaged plasma velocity and the heavy particle temperature. In the following, the length scale $L = 2$ cm is the minimum distance between the diffuser walls. Other scales include T_0, n_0, and $p_0 = n_0 k T_0$. The ionization degree is multiplied by factor of 10^4, and the electric conductivity is presented in mho/m.

Figures 8a–8f display the flow structure in the MHD section without an applied magnetic field. The results demonstrate a significant variation of plasma parameters along the MHD section of the experimental setup. It is seen that the flow under study remains essentially nonequilibrium down to the outlet of the MHD section, which is evidenced by the difference between the electron and heavy particle temperatures. Also note the relatively slow decrease of the electron temperature in the nozzle and its relatively small increase within the shocks as compared with the behavior of the heavy particle temperature. The former is explained by energy input into the electron component due to recombination, whereas the latter is explained by higher sound speed and, consequently, by less shock intensity for the electron component. Distributions of the ionization degree and the electric conductivity demonstrate a direct correlation with the flowfield structure.

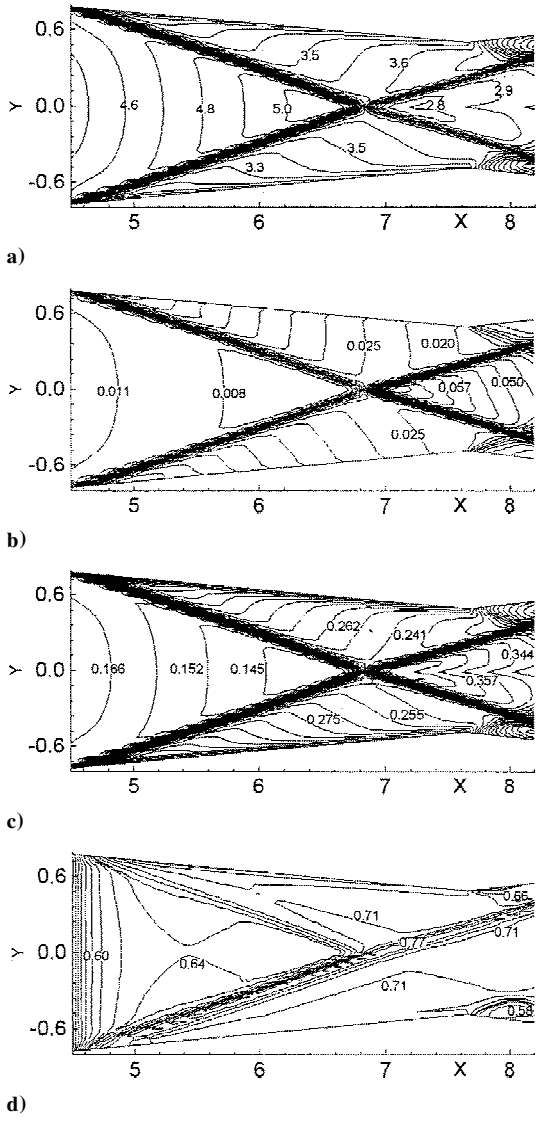

Fig. 9 Contours of a) Mach number, b) static pressure, c) heavy particle temperature, and d) electron temperature of the plasma at $B = 1.0$ T.

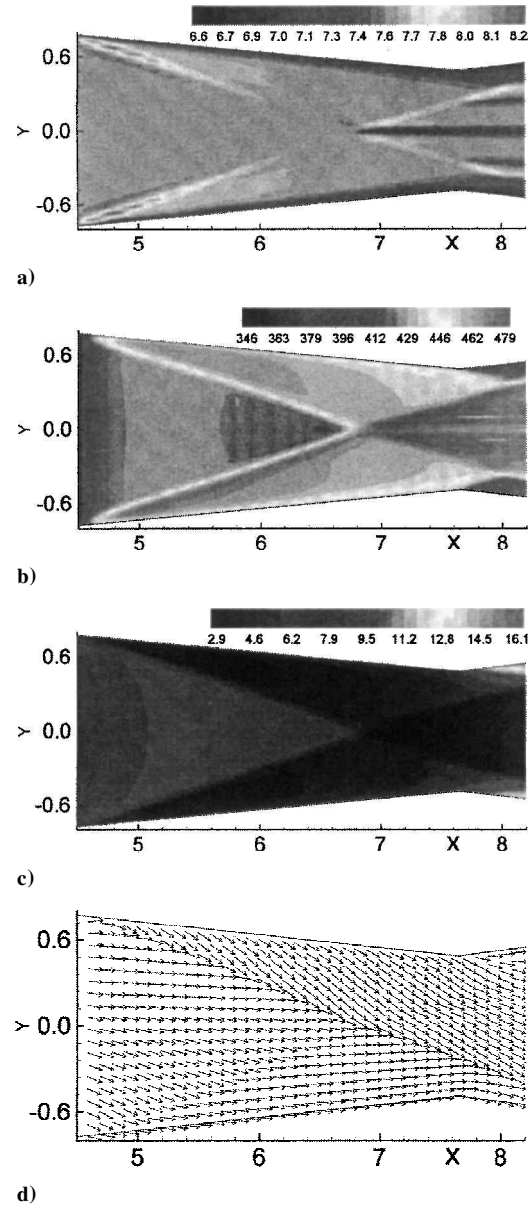

Fig. 10 Contours of a) ionization degree, b) electric conductivity, c) Hall parameter, and d) electric current map of the plasma at $B = 1.0$ T.

The following presents calculations of MHD flows in the diffuser model. Like earlier calculations, the magnetic field is assumed to be aligned with the z axis, as was the case for Fig. 1. The diffuser is considered a Faraday generator with continuous electrodes and the external load coefficient, $k = 0.5$. Figures 9 and 10 display distributions of plasma parameters in the diffuser model at the induction of applied magnetic field, $B = 1$ T. Comparison with earlier examples reveals a weak deceleration of plasma flow by the applied magnetic field, which is explained by high values of the Hall parameter reaching a maximum in the expansion fans near the diffuser outlet. The Hall effect is responsible for the electric current direction shown in Fig. 10d. Drastic influence of the Hall current on flowfield structure and plasma deceleration is demonstrated by comparison with the results shown in Fig. 11, which presents calculations made while the Hall effect was ignored. In this case, the applied magnetic field decelerates the plasma flow down to subsonic speed. The Mach number contours reveal the normal shock followed by a small subsonic zone. These results show that a segmented electrode is required to suppress the Hall current in situations where moderate-to-large Hall parameters are realized.

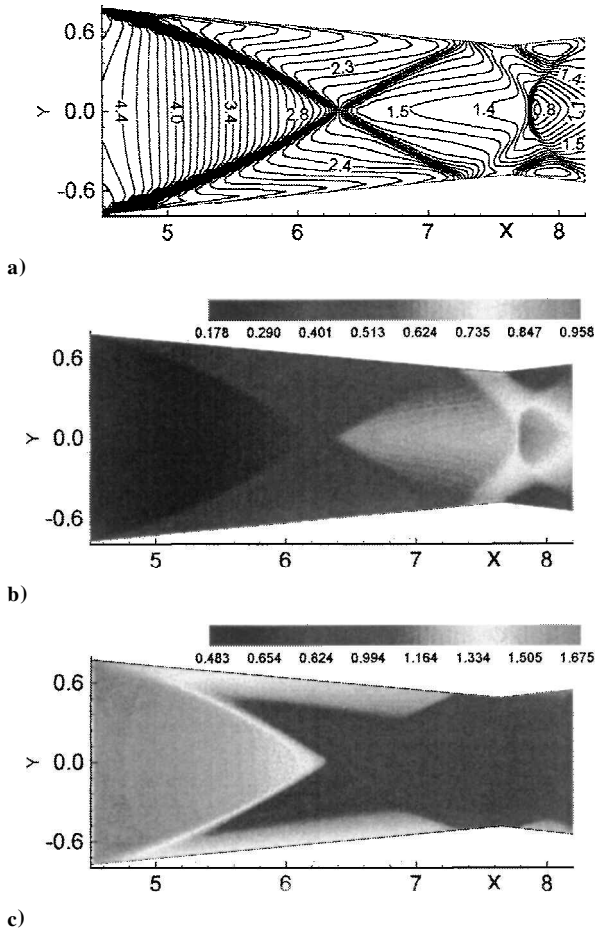

Fig. 11 Contours of a) Mach number, b) heavy particle temperature, and c) electron temperature in the diffuser model at $B = 1.0$ T, given $\beta_e = 0.0$.

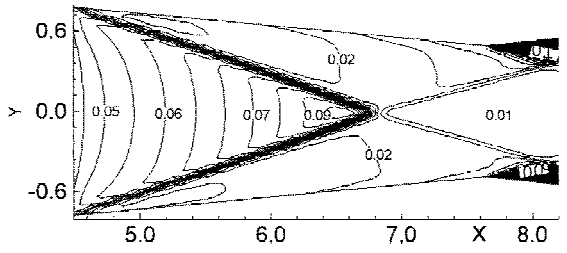

Fig. 12 Contours of ion slip parameter at $B = 1.0$ T.

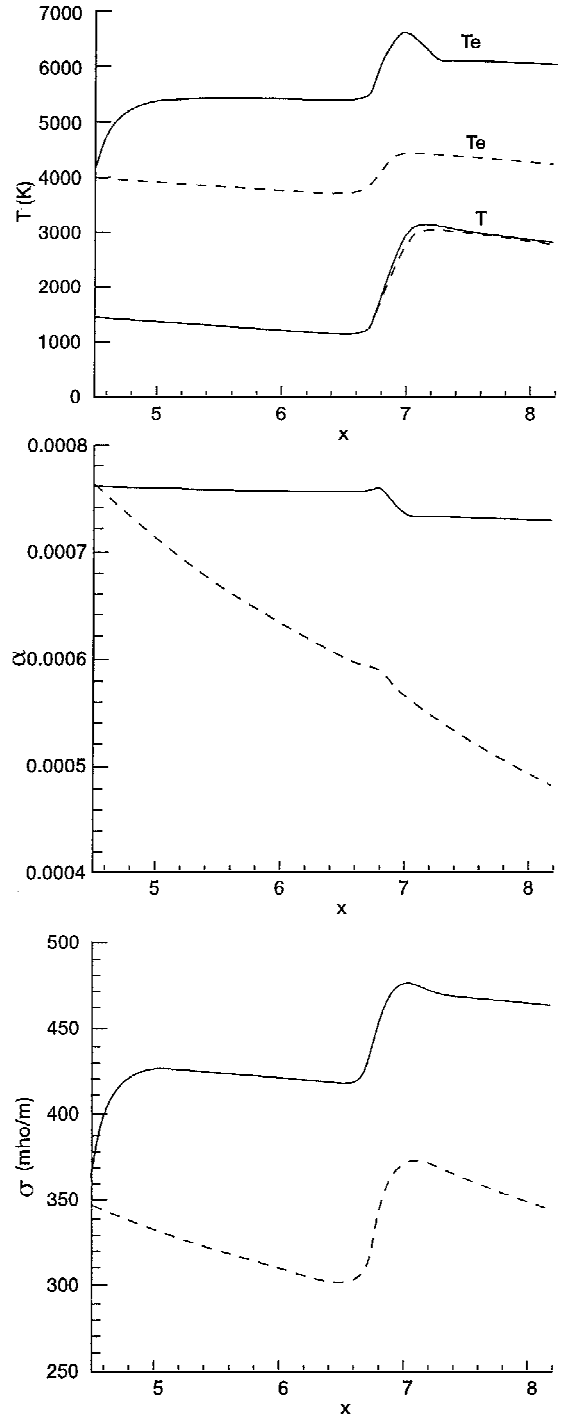

Fig. 13 Variation of plasma parameters along the symmetry plane of the diffuser model: ——, $B = 1.0$ T and - - - -, $B = 0.0$.

It is also of interest to estimate the ion slip effect. With that end in view, the ion slip parameter $s = (\rho_a/\rho)^2 \beta_e \beta_i$ was evaluated, where β_i is the Hall parameter for ions. The results are presented in Fig. 12. When the collision frequency of ions and atoms is evaluated, which is required to calculate β_i, the cross section σ_{ia} was assumed to be equal to 5×10^{-19} m^2, in accordance with the data presented in Ref. 10 for the charge exchange between ions and atoms of argon. The results of Fig. 12 indicate a negligible role of the ion slip in the flows under study.

Figure 13 presents distributions of plasma parameters along the symmetry plane of the diffuser model. Solid and dashed curves correspond to flows with and without an applied magnetic field. It is seen in Fig. 13 that the heavy particle temperature is only slightly affected by the applied magnetic field, whereas the electron temperature is significantly increased. Also note a substantial increase in the ionization degree and the electric conductivity due to the applied magnetic field.

Conclusions

Numerical investigation of MHD flows in the model of a supersonic intake has been carried out. The results of numerical simulation provide evidence of the possibility of plasma flow deceleration down to subsonic speed by application of a magnetic field; however, the results also indicate a substantial total pressure loss inherent in such a mode of flow control. The results also demonstrate that a desirable change in the flow structure may be produced by local use of the MHI. The calculations of plasma flows in the MHD section of the experimental setup provide evidence that the flows under study are essentially nonequilibrium, having an ionization degree and an electric conductivity higher than those without a magnetic field. Plasma deceleration by an applied magnetic field in a Faraday-type device becomes more effective with suppression of the Hall effect, which

may be achieved by segmentation of the electrodes. Excessive MHI results in such undesirable phenomena as flow separation and production of a nonstationary flow regime associated with flow choking.

References

[1]Gurijanov, E. P., and Harsha, P. T., "AJAX: New Directions in Hypersonic Technology," AIAA Paper 96-4609, Nov. 1996.

[2]Fraishtadt, V. L., Kuranov, A. L., and Sheikin, E. G., "Use of MHD Systems in Hypersonic Aircraft," *Technical Physics*, Vol. 43, 1998, p. 1309.

[3]Golovachov, Yu. P., Il'in, S. A., and Sushchikh, S. Yu., "Magnetic Field Control of Gas Flow in a Supersonic Intake," Technical Physics Letters, Vol. 23, No. 8, 1997, pp. 615–616.

[4]Vatazhin, A. B., Kopchenov, V. I., and Gouskov, O. V., "Some Estimation of Possibility to Use the MHD Control for Hypersonic Flow Deceleration," AIAA Paper 99-4972, July 1999.

[5]Golovachov, Yu. P., Sushchikh, S. Yu., and Van Wie, D. M., "Numerical Simulation of MGD Flows in Supersonic Inlets," Paper AIAA-2000-2666, June 2000.

[6]Macheret, S. O., Shneider, M. N., and Miles, R. B., "Potential Performance of Supersonic MHD Power Generators," AIAA Paper 2001-0795, Jan. 2001.

[7]Munipalli, R., and Shankar, V., "Development of Computational Capabilities in Real Gas MHD," AIAA Paper 2001-0198, Jan. 2001.

[8]Park, Ch., Bogdanoff, D. W., and Mehta, U. B., "Theoretical Performance of a Nonequilibrium MHD-Bypass Scramjet," AIAA Paper 2001-0794, Jan. 2001.

[9]Vasil'eva, R. V., Genkin, A. L., Goryachov, V. L., Erofeev, A. V., Zuev, A. D., Mirshanov, D. N., Renennuyi, A. S., and Silin, N. A., "Low-Temperature Plasma of Noble Gases with Non-Equilibrium Ionization and MHD Generators," Ioffe Physico-Technical Inst., St. Petersburg, Russia, 1991 (in Russian).

[10]Biberman, L. M., Vorob'ev, V. S., and Yakubov, I. T., *Kinetics of Low-Temperature Non-Equilibrium Plasma*, Nauka, Moscow, 1982 (in Russian).

[11]Mitchner, M., and Kruger, C. H., Jr., *Partially Ionized Gases*, Wiley, New York, 1973.

[12]Volkov, Yu. M., Zinov'ev, O. A., and Maluta, D. D., "Measurement of the Diffusion Cross-Sections of Low-Energy Electrons in Rare Gases Using the Microwave Technique," *Teplofizika Vysokikh Temperature*, Vol. 6, No. 2, 1963, pp. 209–218 (in Russian).

[13]Breyev, V. V., Gubarev, A. V., and Punchenko, V. P., *Supersonic MHD Generators*, Energoatomizdat, Moscow, 1988 (in Russian).

[14]Rodionov, A. V., "Improvement of Accuracy of S. K. Godunov's Scheme," *Zhurnal Vychislitenoi Matematiki I. Matematicheskoi Fiziki*, Vol. 27, No. 12, 1989, pp. 1853–1860.

[15]Roache, P., *Computational Fluid Dynamics*, Hemisphere, New York, 1978.

[16]Bobashev, S. V., D'yakonova, E. A., Erofeev, A. V., Lapushkino, T. A., Maslennikov, V. G., Poniaev, S. A., Sacharov, A. A., Vasil'eva, R. V., and Vanwie, D. M., "Shock-Tube Facility for MGD Supersonic Flow Control," AIAA Paper 2000-2647, June 2000.

[17]Vatazhin, A. B., Gouskov, O. V., Kopchenov, V. I., and Likhter, V. A., "On the Problem of Deceleration of Electrically Conducting Supersonic Flows in the Ducts by a Magnetic Field," *Izvestiya Rossiiskoy Akodemii Nauk. Mechanika Zhid kosti i Gaza*, No. 5, 1998, pp. 169–181.